Appl. Phys. B 38, 219–224 (1985)

Applied Physics B Photophysics and Laser Chemistry

Laser-Induced Reactions of NO_2 in the Visible Region

I. Kinetic Modeling of Nitrobutane Formation in the NO_2-Isobutane System

M. E. Umstead, S. A. Lloyd*, J. W. Fleming, and M. C. Lin

Chemistry Division, Naval Research Laboratory, Washington, DC, WA 20375-5000, USA

Received 18 June 1985/ Accepted 17 August 1985

Abstract. The reaction of NO_2 with isobutane, induced by 488 nm laser radiation, to form 2-nitro-2-methylpropane has been investigated and the results computer-modeled according to two possible reaction mechanisms. The first scheme involves the direct abstraction of H from isobutane by vibronically excited NO_2 ($NO_2^{*\dagger}$), and the second, abstraction by an intermediate NO_3 radial produced by $NO_2^{*\dagger} + NO_2$. The modeling results strongly support the $NO_2^{*\dagger}$ scheme as the dominant reaction mechanism.

PACS: 82.30, 82.50

We have found that 2-nitro-2-methylpropane is formed when NO_2 is irradiated with the lines from an argon-ion laser in the presence of isobutane. A preliminary account of this work has been published [1]. Further work has now been carried out on this reaction, and the experimental results have been kinetically modeled with a computer to elucidate the reaction mechanism.

At the wavelengths emitted by an argon-ion laser (457.9–514.5 nm), NO_2 does not dissociate to form O atoms, the usual initiators of photochemical nitration reactions. Sato and Cvetanovic determined the long-wavelength limit of the photooxidation of 1-butene by NO_2 and found products of the reaction of O atoms with butene in the presence of the 404.7 nm Hg line, but none with the very intense 435.8 nm line [2]. Based on bond energies the theoretical limit for the dissociation of NO_2 into NO and O atoms is <400 nm. The photodissociation at 404.7 nm can be explained by contributions from the vibrational and rotational energies of the molecule [3].

Two plausible reaction mechanisms can be postulated to explain the reactivity of NO_2 excited by an argon-ion laser. One of these ($NO_2^{*\dagger}$ scheme) involves the direct abstraction of hydrogen from the hydrocarbon by vibronically excited NO_2 ($NO_2^{*\dagger}$), the other (NO_3 scheme) requires the abstraction by an intermediate NO_3 radical formed by the reaction of $NO_2^{*\dagger}$ with NO_2. Herman et al. reported that the laser-induced oxidation of CO by NO_2 proceeded by the direct reaction of $NO_2^{*\dagger}$ with CO [4]. The NO_3 radical has been postulated to be an important intermediate in the high-temperature nitration of hydrocarbons [5]. The rates of 2-nitro-2-methylpropane (t-$C_4H_9NO_2$) formation and NO_2 disappearance observed in this study as functions of reaction time, laser power, reactant concentration, and quenching by added gases have been computer-modeled according to both mechanisms to see if one could be uniquely chosen over the other on this basis.

1. Experimental

Experimental details have been given in [1]. Briefly, mixtures of NO_2, i-C_4H_{10}, and in some experiments added NO, O_2, or He, were irradiated in a Pyrex cell, 53 cm long by 1 cm ID, enclosed by Pyrex windows at

* Federal Junior Fellow (1980–1984)

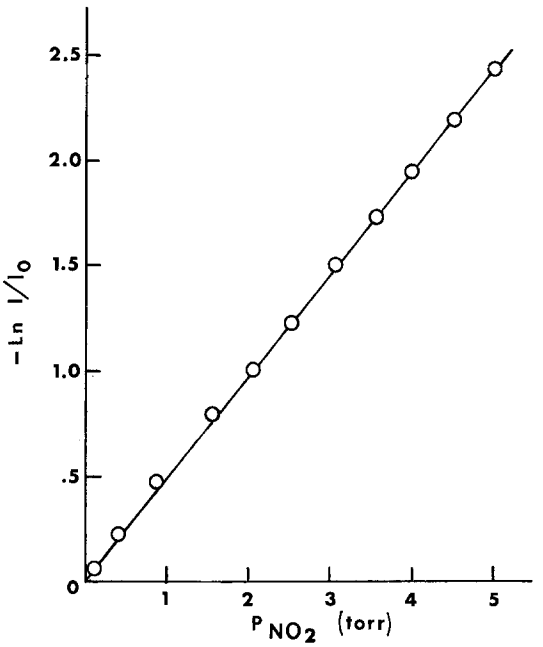

Fig. 1. Beer-Lambert plot of NO_2 absorption of laser beam. (Cell length: 52 cm, 488 nm, 1 W)

each end and equipped with greaseless stopcocks. The beam from a Coherent Model 52 argon-ion laser was directed along the axis of the cell. Most experiments were carried out with the 488 nm line at 1 W.

A linear Beer-Lambert plot (Fig. 1) was obtained with this line with NO_2 pressures up to at least 5 Torr in the cell, so NO_2 concentrations could be determined from the transmitted laser power. After a sample had been irradiated, usually for 15–20 min, the contents of the cell were expanded into a large, low-pressure gas sampling loop in a gas chromatograph and analyzed for organic products.

All gases were obtained from Matheson. The NO_2 was purified by trap-to-trap distillation at 195 K to remove traces of N_2O_3. The NO was passed through a trap at 159 K to remove NO_2 and was then degassed at 77 K. The other gases were used without further purification.

2. Computer Modeling of Reaction Schemes

All probable reactions for both the $NO_2^{*\dagger}$ and NO_3 schemes were computer modeled in order to determine whether one of these mechanisms could be selected unequivocally over the other on this basis. The only reaction product modeled was t-$C_4H_9NO_2$ because of the lack of kinetic data for reactions involving other products. It was assumed that the branching ratios for the formation of t-$C_4H_9NO_2$ and other primary products remained constant, and that most of the secondary products arose from products other than t-$C_4H_9NO_2$, such as nitrites [6].

Initially the NO_2 disappearance curves obtained from the photolysis of pure NO_2 and mixtures of it with added NO and O_2 were modeled according to the following equations:

$$NO_2 + h\nu \rightarrow NO_2^{*\dagger}, \quad (1)$$

$$NO_2^{*\dagger} \rightarrow NO_2 + h\nu, \quad (2)$$

$$NO_2^{*\dagger} + NO_2 \rightarrow 2NO_2, \quad (3)$$

$$NO_2^{*\dagger} + NO_2 \rightarrow 2NO + O_2, \quad (4)$$

$$NO_2^{*\dagger} + O_2 \rightarrow NO_2 + O_2, \quad (5)$$

$$NO_2^{*\dagger} + NO \rightarrow NO_2 + NO, \quad (6)$$

$$2NO + O_2 \rightarrow 2NO_2. \quad (7)$$

The concentrations of the various species involved in the reaction were calculated as a function of time by integrating the coupled differential equations by means of Treanor's modification of a fourth-order Runge-Kutta method [7] with the aid of a Texas Instruments ASC computer.

The rate constants for reactions (3–5) and (7) have been determined, and their values and sources are listed in Table 1. The values used for $NO_2^{*\dagger}$ quenching by NO_2 and O_2 were those reported in [8, 10] for the quenching of the $NO_2^{*\dagger}$ continuum. Reaction (2) can be neglected since the collisionally induced decay time of $NO_2^{*\dagger}$ is much shorter than that for fluorescence [3]. No rate constant for reaction (6) has been reported.

The rate of NO_2 excitation k_1, which is proportional to the number of photons absorbed, was first varied in the computer until the computed curves closely fit the

Table 1. Reaction rate constants used in and derived from this study. Units are in ml mole^{-1} s^{-1}

Reaction	This work	Literature	Ref.
(3)	[a]	6.8×10^{13}	[8]
(4)	[a]	2.5×10^{10}	[9]
(5)	3.1×10^{13}	3.3×10^{13}	[10]
(6)	6.8×10^{13}		
(7)	[a]	7.1×10^{9}	[11]
(8)	1.2×10^{14}		
(10)	2.9×10^{13}	2.1×10^{13}	[10]
(14)	[a]	1.1×10^{13}	[12]
(15)	[a]	4.8×10^{9}	[11]
(18)	[a]	4.0×10^{16} [b]	[11]
(19)	[a]	5.5×10^{12}	[11]
(20)	[a]	3.6×10^{16} [b]	[11]
(21)	[a]	6.0×10^{10}	[13]
(22)	[a]	2.0×10^{12}	[11]
(23)	[a]	1.0×10^{18} [b]	[11]
(24)	[a]	2.5×10^{17} [b]	[11]

[a] Literature values used in computations

[b] ml^2 mol^{-2} s^{-1}

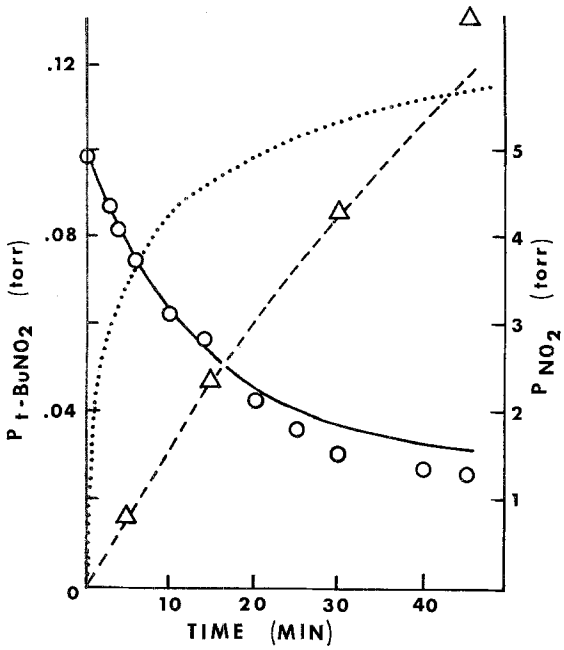

Fig. 2. 2-nitro-2-methylpropane production (left scale) and NO_2 disappearance (right scale) vs. reaction time. Circles: experimental NO_2 values; triangles: experimental $C_4H_9NO_2$ values; solid line: computed NO_2 curve; dashed line: computed $C_4N_9NO_2$ curve, $NO_2^{*\dagger}$ scheme; dotted line: computed $C_4H_9NO_2$ curve, NO_3 scheme. (10 Torr 1:1 NO_2:C_4H_{10}, 1 W)

experimental NO_2 decay points obtained from the 1 W photolysis of pure NO_2 at pressures from 1 to 5 Torr. These results were similar to the NO_2 disappearance curve shown in Fig. 2. Initially, a reasonable value for k_6 was assumed based upon quenching by a diatomic molecule. The results of the experiments with added NO and O_2 were next modeled by varying k_1, k_6 and slightly adjusting k_5 until the computed curves fit all the experimental results from the various mixtures. The final values obtained for k_5 and k_6 are also listed in Table 1. At this point the rate constants for the first seven reactions were fixed, and further reactions involving isobutane were added according to the two schemes.

2.1. $NO_2^{*\dagger}$ *Scheme*

Reactions (8–12) comprise the remainder of the reactions that were considered in the $NO_2^{*\dagger}$ scheme, where RH represents isobutane:

$$NO_2^{*\dagger} + RH \rightarrow NO_2 + RH, \quad (8)$$

$$NO_2^{*\dagger} + RH \rightarrow R + HNO_2, \quad (9)$$

$$NO_2^{*\dagger} + He \rightarrow NO_2 + He, \quad (10)$$

$$R + NO_2 \rightarrow RNO_2, \quad (11)$$

$$R + NO \rightarrow RNO. \quad (12)$$

Of these reactions only the rate constant for reaction (10) has been reported. Rate constants for reactions (11, 12) were estimated to be 6.2×10^{11} and 1.4×10^{11}, respectively, from the data reported by Pratt and Veltman [14] for the methyl and ethyl radicals. Values for k_8 and k_9 were then varied in the computer until a fit was obtained with the experimental points from a series of experiments in which the initial isobutane concentration was varied. Fortunately, the modeling is not sensitive to the absolute rate constants for reactions (9, 11, and 12) since (9) is coupled with the other two. The rates of (11, 12) can be varied over a wide range without significantly affecting the computed curves so long as the rate of reaction (9) is modified accordingly. Finally, k_{10} was adjusted to fit the computed curve to the experimental one obtained from the He quenching experiments; the values obtained are listed in Table 1.

2.2. NO_3 *Scheme*

The following reactions were added to the initial seven to model the reaction according to the NO_3 scheme:

$$NO_2^{*\dagger} + RH \rightarrow NO_2 + RH, \quad (8)$$

$$NO_2^{*\dagger} + He \rightarrow NO_2 + He, \quad (10)$$

$$NO_2^{*\dagger} + NO_2 \rightarrow NO_3 + NO, \quad (13)$$

$$NO_3 + NO \rightarrow 2NO_2, \quad (14)$$

$$NO_3 + NO_2 \rightarrow NO + O_2 + NO_2, \quad (15)$$

$$NO_3 + RH \rightarrow R + HNO_3, \quad (16)$$

$$R + NO_2 \rightarrow RNO_2, \quad (11)$$

$$R + NO \rightarrow RNO. \quad (12)$$

Reactions (17–24) take into account the initiation of the reaction by O atoms produced by the photolysis of NO_3:

$$NO_3 + h\nu \rightarrow NO_2 + O, \quad (17)$$

$$O + NO + M \rightarrow NO_2 + M, \quad (18)$$

$$O + NO_2 \rightarrow NO + O_2, \quad (19)$$

$$O + NO_2 + M \rightarrow NO_3 + M, \quad (20)$$

$$O + RH \rightarrow R + OH, \quad (21)$$

$$OH + RH \rightarrow R + H_2O, \quad (22)$$

$$OH + NO_2 + M \rightarrow HNO_3 + M, \quad (23)$$

$$OH + NO + M \rightarrow HNO_2 + M. \quad (24)$$

NO_3 has been reported by Graham and Johnston to photodissociate into O atoms and NO_2 at wavelengths shorter than 580 nm [12]. They measured

a cross section of 4.8×10^5 cm^2 mole^{-1} for the photodissociation at 488 nm, and this value was used in these computations.

The rates of all these reactions except (13 and 16) were either available in the literature at the time the modeling was carried out or have been evaluated earlier in this study (Table 1). It was assumed that the rate of reaction (16) would not exceed the reaction rate of O atoms with i-C_4H_{10}, 6.1×10^{10} [15], based on data reported for the rate of reaction of NO_3 with some olefins [13]. A value of 6×10^{10} (equal to k_{21}) was initially assigned to k_{16}, and k_{13} was varied to compute the rate of t-$C_4H_9NO_2$ formation as a function of time. The absolute values chosen for the rate constants for reactions (13, 16), the rate of formation of NO_3 and its loss through reaction with i-C_4H_{10}, proved to be non-critical as the two reactions are coupled. Values for k_{13} could be varied over a range of at least 100 without significantly changing the predicted t-$C_4H_9NO_2$ formation curve so long as k_{16} was varied accordingly in the opposite direction. The upper limit for k_{13} was found to be approximately 2×10^{12}. Computations based upon values greater than that caused the computed NO_2 disappearance curves to move away from the experimental one. Since this work was carried out, k_{16} has been measured to be 1.6×10^7 [16], which is outside the range over which k_{13} and k_{16} could be varied and still fit the experimental NO_2 disappearance.

No fit of the computed curves with the experimental data could be obtained with the NO_3 scheme. Computations over the entire range of values chosen for k_{13} and k_{16} predicted marked curvature in the t-$C_4H_9NO_2$ formation curve, while the experimental one was close to linear. Even though no definite rate constants for these reactions could be obtained from the NO_3 scheme, further computations were carried out for experiments in which the initial NO_2 and i-C_4H_{10} were varied, and for the experiments on the effects of some added gases. For these calculations k_{13} was set at 4×10^{10} and k_{16} was varied to attempt to fit the computed curves to the experimental results.

The photodissociation of NO_3 and the subsequent reactions of the O atoms produced proved to be of no consequence in the reaction mechanism. Reactions (17–24) could be dropped from the scheme without at all affecting the computed results.

3. Results and Discussion

Figure 2 shows the experimental rates of NO_2 disappearance and t-$C_4H_9NO_2$ production during the photolysis of a mixture of NO_2 and i-C_4H_{10} as well as the computed rates by both the $NO_2^{*\dagger}$ and NO_3 mechanisms. The computed $NO_2^{*\dagger}$ curve agrees well with the experimental data. No fit could be obtained with the NO_3 scheme. Similar results, shown in Fig. 3, were obtained when the laser power was varied. The t-$C_4H_9NO_2$ production was linear with power while the NO_3 model predicts marked curvature. Laser power was varied in the modeling by varying the incident intensity (I_0) in computing the NO_2 excitation rate. The linear t-$C_4H_9NO_2$ production is indicative of a reaction proceeding by a single photon process.

The marked curvature predicted by the NO_3 scheme can be explained by considering reaction (14). NO reacts very rapidly with NO_3 to form NO_2, $k_{14} = 1.1 \times 10^{13}$. Thus as NO builds up in the system mainly *via* reaction (4), the NO_3 steady-state concentration is rapidly depleted, slowing down reaction (16). To test this hypothesis, the effect of varying amounts of added NO were modeled. As expected, the NO_3 mechanism predicted a rapid decrease in t-$C_4H_9NO_2$ formation with added NO, while the $NO_2^{*\dagger}$ scheme predicted only a gradual decrease (Fig. 4). The latter mechanism provided a good fit with the experimental data. In an experiment at higher NO_2 and i-C_4H_{10} pressures, the photolysis of 5 Torr each of these in the presence of added NO was found to produce more t-$C_4H_9NO_2$ than could be accounted for by either mechanism. The reason for this is not known.

Figure 5 shows the effect of varying the initial NO_2 pressure on t-$C_4H_9NO_2$ production. The computed

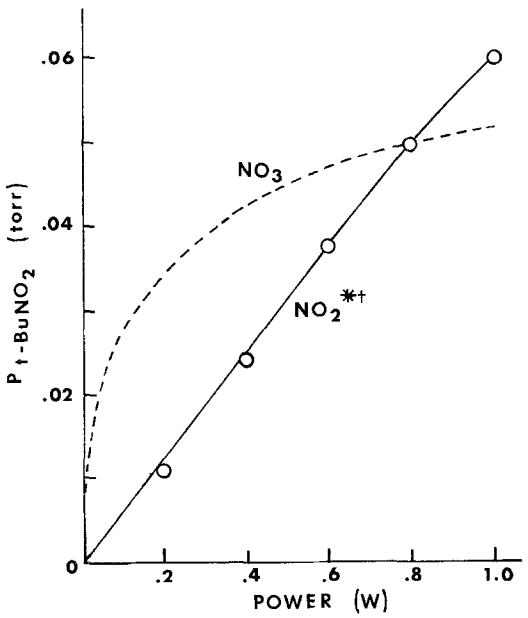

Fig. 3. 2-nitro-2-methylpropane production vs. laser power. Circles: experimental points; solid curve: computed by $NO_2^{*\dagger}$ scheme; dashed curve: computed by NO_3 scheme. (10 Torr 1 : 1 NO_2 : C_4H_{10}, 20 min)

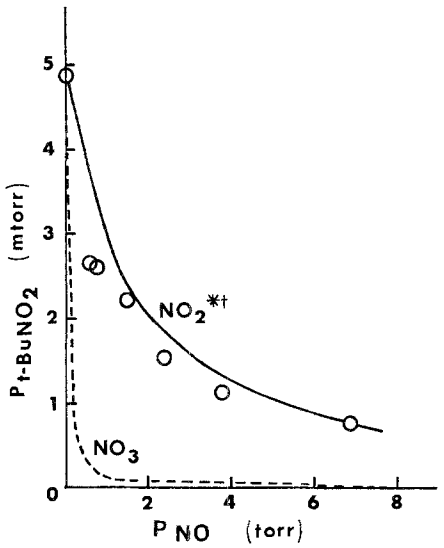

Fig. 4. 2-nitro-2-methylpropane formation vs. added NO pressure. Circles: experimental points; solid curve: computed by $NO_2^{*\dagger}$ scheme; dashed curve: computed by NO_3 scheme. (x Torr NO, 0.5 Torr NO_2, 5 Torr C_4H_{10}, 1 W, 20 min)

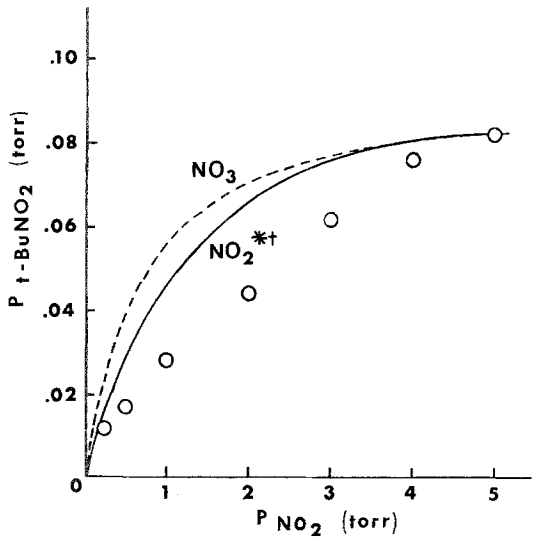

Fig. 5. 2-nitro-2-methylpropane formation vs. initial NO_2 pressure. Circles: experimental points; solid curve: computed by $NO_2^{*\dagger}$ scheme; dashed curve: computed by NO_3 scheme. (x Torr NO_2 + 5 Torr C_4H_{10}, 1 W, 20 min)

curves (constrained to fit the experimental point at 5 Torr NO_2 by adjusting k_9 and k_{16}) were similar for both mechanisms and showed more curvature than the experimental points. No choice between the two mechanisms could be made on the basis of this experiment.

Figure 6 illustrates the effect of varying the initial i-C_4H_{10} pressure. The $NO_2^{*\dagger}$ mechanism provided good agreement with the experimental points while the

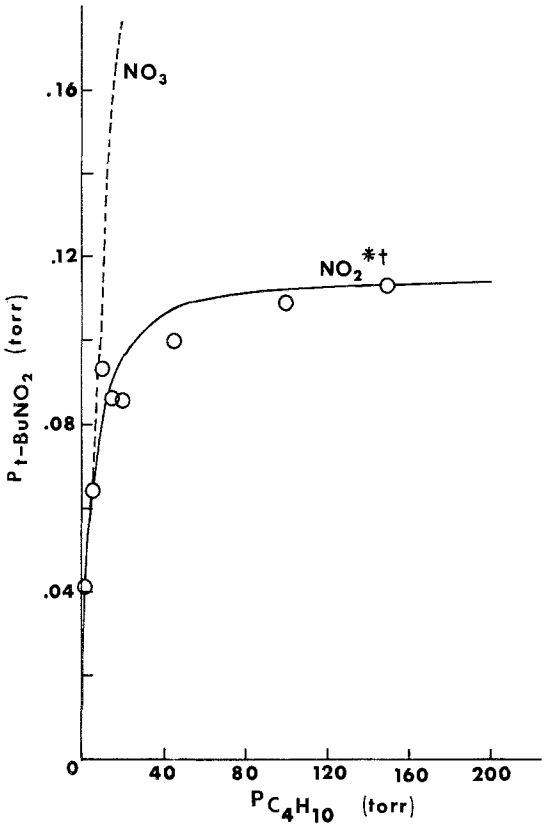

Fig. 6. 2-nitro-2-methylpropane formation vs. initial i-C_4H_{10} pressure. Circles: experimental points; solid curve: computed by $NO_2^{*\dagger}$ scheme; dashed curve: computed by NO_3 scheme. (x Torr C_4H_{10} + 5 Torr NO_2, 1 W, 20 min)

NO_3 scheme did not. The i-C_4H_{10} quenching rate, k_8, computed by the $NO_2^{*\dagger}$ scheme was 1.2×10^{14}, a value slightly higher than that reported by Haaks and Schurath for the quenching of the $NO_2^{*\dagger}$ continuum by 1-butene, 8.4×10^{13} [17]. However, they also found a lower rate for NO_2 than did Keil, Donnelly, and Kaufman [8]. The relative rate of i-C_4H_{10} and NO_2 quenching, k_8/k_3, found in this study was 1.8, and agreed well with the ratio of 1.9 obtained from the data of Haaks and Schurath for 1-butene.

Figure 7 shows the effect of added He as an $NO_2^{*\dagger}$ quencher. The $NO_2^{*\dagger}$ scheme provided good agreement with the data when a fitted k_{10} of 2.9×10^{13} is used, which is in fair agreement with that found by Donnelly et al. (Table 1). The computed curve for the NO_3 scheme shown in the figure is based upon the same value and lies considerably above the experimental points. The NO_3 curve can be made to fit the experimental data by the use of a value of 4×10^{14} for k_{10}. This number, however, is unreasonably large.

Computer-modeling of our experimental results clearly supports the $NO_2^{*\dagger}$ scheme as the dominant mechanism for the laser-induced reaction of NO_2 with iso-

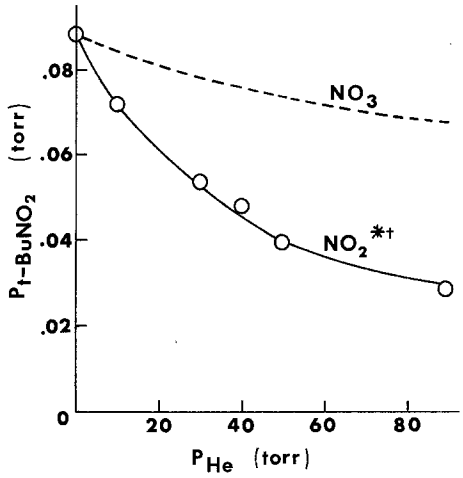

Fig. 7. 2-nitro-2-methylpropane formation vs. added He pressure. Circles: experimental points; solid curve: computed by $NO_2^{*\dagger}$ scheme; dashed curve: computed by NO_3 scheme. (x Torr He, 5 Torr NO_2, 5 Torr C_4H_{10}, 1 W, 20 min)

butane. Only in the one instance in which the partial pressure of NO_2 was varied did the modeling not show a clear preference between these two mechanisms. Our subsequent study of the laser-induced reaction of NO_2 with CO also indicates a similar mechanism involving $NO_2^{*\dagger}$ for that reaction [18].

4. Summary

The laser-induced reaction of NO_2 with i-C_4H_{10} has been investigated and the results computer-modeled. The modeling of the yield of the key nitration product, t-$C_4H_9NO_2$, as a function of reaction time, laser power, i-C_4H_{10} pressure, and the effect of added gases such as NO and He all support a mechanism in which the reaction takes place by direct hydrogen abstraction by vibronically excited NO_2 rather than by an intermediate NO_3 radical.

References

1. M.E. Umstead, J.W. Fleming, M.C. Lin: IEEE J. QE-**16**, 1227 (1980)
2. S. Sato, R.J. Cvetanovic: Can. J. Chem. **36**, 279 (1958)
3. J.G. Calvert, J.N. Pitts, Jr.: *Photochemistry* (Wiley, New York 1966) p. 219
4. I.P. Herman, R.P. Mariella, A. Javan: J. Chem. Phys. **68**, 1070 (1978)
5. A. Titov: Tetrahedron **19**, 557 (1963)
6. G. Paraskelopoulos, R.J. Cvetanovic: J. Phys. Chem. **81**, 2598 (1977)
7. C.E. Treanor: Math. Computation **20**, 39 (1966)
8. D.J. Keil, V.M. Donnelly, F. Kaufman: J. Chem. Phys. **73**, 1514 (1980)
9. C.L. Creel, J. Ross: J. Chem. Phys. **64**, 3560 (1976)
10. V.M. Donnelly, D.J. Keil, F. Kaufman: J. Chem. Phys. **71**, 659 (1979)
11. NBS Special Publication 513, *Reaction Rate and Photochemical Data for Atmospheric Chemistry – 1977*, pp. 27, 40, 1978
12. R.A. Graham, H.S. Johnston: J. Phys. Chem. **82**, 254 (1978)
13. S.M. Jarpar, H. Niki: J. Phys. Chem. **79**, 1629 (1975)
14. G. Pratt, I. Veltman: Faraday Trans. I **72**, 2477 (1976)
15. N. Washida, K.D. Bayes: J. Phys. Chem. **84**, 1309 (1980)
16. R. Atkinson, C.N. Plum, W.P.L. Carter, A.M. Winer, J.N. Pitts: J. Chem. Phys. **88**, 2361 (1984)
17. D. Haaks, U. Schurath: In *Laser-Induced Processes in Molecules*, ed. by K.L. Kompa and S.D. Smith, Springer Ser. Chem. Phys. **6** (Springer, Berlin, Heidelberg 1979) p. 352
18. M.E. Umstead, S.A. Lloyd, M.C. Lin: Appl. Phys. B **39** (to be published, 1986)